Cancer Letters 454 (2019) 108–119

Contents lists available at ScienceDirect

Cancer Letters

journal homepage: www.elsevier.com/locate/canlet

Original Articles

Combined class I histone deacetylase and mTORC1/C2 inhibition suppresses the initiation and recurrence of oral squamous cell carcinomas by repressing SOX2

Xueyi Liang[a,b,1], Miao Deng[a,b,1], Chi Zhang[a,b,1], Fan Ping[a,b], Hongfei Wang[a,b], Yun Wang[b], Zhaona Fan[b], Xianyue Ren[b], Xiaoan Tao[a,b], Tong Wu[a,b], Jian Xu[c], Bin Cheng[a,b,*], Juan Xia[a,b,**]

[a] Department of Oral Medicine, Guanghua School of Stomatology, Sun Yat-sen University, Guangzhou, PR China
[b] Guangdong Provincial Key Laboratory of Stomatology, Guanghua School of Stomatology, Sun Yat-sen University, Guangzhou, PR China
[c] Center for Craniofacial Molecular Biology, School of Dentistry, University of Southern California, Los Angeles, CA, USA

ARTICLE INFO

Keywords:
Cancer stem cells (CSCs)
4SC-202
INK128
Oral cancer

ABSTRACT

Treatment of oral squamous cell carcinoma (OSCC) remains a challenge because of the lack of effective early treatment strategies and high incidence of relapse. Here, we showed that combined 4SC-202 (a novel selective class I HDAC inhibitor) and INK128 (a selective mTORC1/C2 inhibitor) treatment exhibited synergistic effects on inhibiting cell growth, sphere-forming ability, subcutaneous tumor formation and ALDH1$^+$ cancer stem cells (CSCs) in OSCC. The initiation of OSCC was significantly inhibited by combined treatment in 4NQO-induced rat model. In addition, upregulated SOX2 was associated with advanced and metastatic tumors in OSCC patients and was responsible for the drug-resistance property of OSCC cells. The inhibitory effect of combined treatment on cell viability and ALDH1$^+$ CSCs were attenuated by SOX2 verexpression. Furthermore, combined treatment can effectively overcome chemoresistance and inhibit the growth of recurrent OSCC *in vitro* and *in vivo*. Mechanistically, 4SC-202 and INK128 repressed SOX2 expression through miR-429/miR-1181-mediated mRNA degradation and preventing cap-dependent mRNA translation, respectively. These results suggest that combined class I histone deacetylase and mTORC1/C2 inhibition suppresses the carcinogenesis and recurrence of OSCC by repressing SOX2.

1. Introduction

Oral cancer is one of the most common cancers worldwide, with an annual incidence of approximate 600,000 [1,2]. Oral squamous cell carcinoma (OSCC) accounts for approximately 90% of oral cancers. OSCC is characterized by aggressive loco-regional invasion, high rate of early recurrences and poor prognosis [3]. Since most OSCCs are diagnosed at locally advanced or metastatic stages [4], the 5-year survival rate is lower than 50% despite advances in combined modality therapy [5]. Currently, cisplatin is the most common chemotherapeutic drug used for OSCC. However, cisplatin treatment has complications of increased cancer stem cells (CSCs), leading to the initiation, drug resistance and relapse of OSCC [6–10]. Effective therapies against OSCC are still elusive.

Epigenetic modifications are associated with tumor progression and drug resistance in OSCC [11]. Histone deacetylases (HDACs) epigenetically represses gene transcription by removing acetyl groups from histones [12], presenting a promising therapeutic target for cancer treatment. Overexpression of class I HDACs is associated with advanced OSCC with poor prognosis [13], while pharmacological inhibition of classes I and II HDAC reduced cell growth and the number of CSCs in OSCC [14]. On the other hand, the PI3K/AKT/mTOR pathway plays a crucial role in regulating cell cycle [15], and more than 80% of head and neck squamous cell carcinoma (HNSCC) presents up-regulation of the PI3K/AKT/mTOR pathway [16,17]. In addition, the persistent activation of the PI3K/AKT/mTOR pathway is associated with resistance or failure of treatment [18]. Furthermore, recurrent HNSCC and chemoresistant cells are susceptible to PI3K/mTOR inhibitor treatment [6,7]. These findings suggest that inhibiting both HDACs and PI3K/AKT/mTOR pathway reduces chemoresistance of OSCC.

** Corresponding author. No.56 Linyuan Xi Road, Guangzhou, Guangdong 510055, China.
* Corresponding author. No.56 Linyuan Xi Road, Guangzhou, Guangdong 510055, China.
E-mail addresses: chengbin@mail.sysu.edu.cn (B. Cheng), xiajuan@mail.sysu.edu.cn (J. Xia).
[1] Equal contribution.

https://doi.org/10.1016/j.canlet.2019.04.010
Received 5 December 2018; Received in revised form 2 April 2019; Accepted 5 April 2019
0304-3835/

In this study, we simultaneously targeted the class I HDAC and mTORC1/C2 by 4SC-202 and INK128 respectively [19–26]. We found a potent synergistic effect in the combined treatment against OSCC with reduced chemoresistance and tumor recurrence. Mechanistically, 4SC-202 repressed SOX2 expression through miR-429/miR-1181-mediated translational repression, while INK128 inhibited SOX2 via preventing cap-dependent mRNA translation. These results identify a promising combination for the development of novel anti-cancer therapeutics in OSCC.

2. Materials and methods

2.1. Cell lines, human OSCC samples and animals

Human OSCC cell lines SCC9, SCC15, SCC25 and CAL27 were obtained from ATCC (Manassas, VA, USA). Human oral cancer cell line KB, and KV which is resistant to the vincristine (VCR),were purchased from cell bank of the animal center of Sun Yat-sen University. Human OSCC cell lines HSC6, CAL33 and normal oral keratinocytes (NOK) were provided by J. Silvio Gutkind (NIH, Bethesda, MD, USA). CAL27R which is resistant to cisplatin and human OSCC cell line UM1, were provided by Jingsong Li (the Second Affiliated Hospital of Sun Yat-sen University). All cell lines were cultured as previously described [27].

Human OSCC samples were obtained from the Department of Craniofacial Surgery and informed consent was obtained from each patient. The study was approved by the Ethics Committee of the Hospital of Stomatology, Sun Yat-sen University.

All 6–8 weeks old rats and NOD/SCID mice were obtained from the Animal Care Unit of Guangdong, China and their care was in accordance with institution guidelines of Sun Yat-sen University. All procedures were performed based on the Sun Yat-sen University Animal Research Committee-approved protocols.

Information regarding the manufacturer, the source for all reagents and antibodies used in this study were listed in Supplementary Table S1.

2.2. Cell proliferation assay and apoptosis assay

Cell proliferation was analyzed using the Cell Counting Kit-8 (CCK-8, Sigma-Aldrich, Santa Clara, CA, USA) and apoptosis was measured using Annexin V FITC Apoptosis Detect Kit (# 556,547, BD, USA) according to the manufacturer's protocol. All experiments were carried out in triplicates.

2.3. Animal model

For 4-Nitroquinoline(4NQO)-induced OSCC model, tongue cancer was induced in rats (female, age 6–8 weeks) by 4NQO (25 μg/mL) in the drinking water for 16 weeks. Rats were randomly divided into 5 groups ($n \geq 8$ for each group) at week 16: vehicle control (p.o. 2% DMSO, 30% PEG 300, 5% Tween 80 and ddH2O), 4SC-202 (60 mg/kg), INK128 (0.2 mg/kg), 60 mg/kg 4SC-202 plus 0.2 mg/kg INK128, or 1 mg/kg cisplatin. At the end of week 22, the rats were sacrificed to obtain the lesions in the tongue tissue.

2.4. Subcutaneous xenogeneic model

The subcutaneous xenogeneic OSCC model was established in immunocompromised mice using the CAL33 cells as previously reported [18]. The mice were randomly divided into four groups ($n \geq 8$ for each group) and treated with vehicle, 4SC-202, INK128 or the combined 4SC-202 and INK128 treatment for 17 days. Subcutaneous tumor growth was monitored every 3 days.

2.5. Recurrent OSCC rat model

Recurrent OSCC rat model was established by two rounds of drug treatment. 4NQO-induced OSCC rat received the first-round treatment with cisplatin from week 22 to week 36, then rats were maintained for an additional 4 weeks. Rats with recurrent lesions were randomly divided into three groups and received a second-round treatment with vehicle, cisplatin or combined 4SC-202 and INK128 for 3 weeks.

2.6. Immunohistochemistry

Immunohistochemistry was performed as previously described [28]. Information of the primary antibodies is listed in Supplementary Table S1. Positive cells were defined as the typical immunostaining. The staining index (SI) for SOX2/ALDH1 was scored according to the staining intensity (0, no staining; 1, weak, light yellow; 2, moderate, yellow brown; 3, strong, brown) and the proportion of positive cells (0, negative; 1, < 10%; 2, < 50%; 3, < 75%; 4, ≥75%) according to the following formula: SI = the proportion of positively stained cells × the staining intensity. Cases with SI (SOX2/ALDH1) > 4 were classified into the high-expression group, and those with SI ≤ 4 were classified into the low-expression group.

2.7. RNA-seq analysis

Next-generation sequencing of paired-end 50 nt reads was performed using the polyA-based libraries at Complete Genomics Company (BGI, Shenzhen, China). The expression level was quantified in reads/kilobase of transcript per million mapped reads (RPKM) using a software package called RSEM. The heatmap was generated using the R language (https://www.r-project.org/). Transcripts with higher than 2-fold change in the expression level were subjected to GO (Gene Ontology, http://wego.genomics.org.cn/cgi-bin/wego/index.pl) or KEGG pathway analysis (http://www.genome.jp/kegg/) to identify functional or pathway enrichment.

2.8. Spheroid formation assay

Cells were seeded in low-adhesion 6-well plates and cultured with serum-free DMEM/F12 (Gibco, USA) supplemented with N2 supplement, human recombinant bFGF (20 ng/mL), and EGF (Gibco, (20 ng/mL). After culture for 1–2 weeks, the number of spheres in each well was counted microscopically and the mean of biological triplicates was used for statistical analysis.

2.9. Limiting dilution assay(LDA)

A total of 2.5×10^6 CAL33 cells were subcutaneously injected into BALB/c mice and given the vehicle control, 4SC-202 (p.o.,100 mg/kg) and/or INK128 (p.o., 0.3 mg/kg) for 2 weeks. Different numbers of cells dissociated from human xenogeneic tumors were mixed with Matrigel and subcutaneously injected into the flank region of nude mice. Tumor-initiating frequency (TIF) was calculated using the ELDA Software (http://bioinf.wehi.edu.au/software/elda).

2.10. ALDH activity

The ALDH activity was measured by using the ALDEFLUOR™ detection kit (StemCell Technology, 01700) according to the manufacturer's instructions. Cells were suspended in ALDEFLUOR staining buffer containing ALDEFLUOR reagent (5 μl/ml) and incubated at 37 °C for 30 min. DEAB (N, Ndiethylaminobenzaldehyde) was used as a negative control for setting gates and data were acquired on CytoFLEX (Beckman Coulter). The data was analyzed using CytExpert software (Beckman Coulter).

2.11. Chromatin immunoprecipitation - qPCR (ChIP-qPCR)

ChIP-qPCR was performed using a ChIP assay kit (Millipore, USA) according to the manufacturer's instructions. Primer sequences were as follows: miR-429 primers, Forward-5′-CTT CCC AGC GAG TCC CAT, reverse 5′-CGT CAT CAT TAC CAG GCA GTA TT; miR-1181 primers, Forward-5′-AGG AAC TCT GTG CTA CTC TGA T, Reverse 5′-GCT GGA ATG TGA GGC TCT ATC; ALDH1A1 primers, Forward-5′-TGC CCT AGG TGT TAC AAA TAA GT, Reverse 5′-GCG TGC CTG AGG ATG ACA TTT CT.

2.12. RNA binding protein immunoprecipitation (RIP) analysis

The Millipore Magna-RIP assay was performed following the manufacturer's protocol (EMD Millipore, USA). Cancer cells were lysed in lysis buffer. Before the IP, protein A/G-agarose beads were washed with RIP Wash Buffer, and incubated with EIF4E antibody, with slow rotation for 30 min at room temperature. Samples were incubated at 4 °C overnight with protein A/G-agarose beads and antibody against EIF4E (cat. No.: MA1-089, MA1-089, Thermo Fisher, USA) or isotype control immunoglobulin G (IgGs, PP64B). Reverse transcription was performed using the Transcriptor First Strand cDNA Synthesis Kit (Roche). For qRT–PCR, 2.5 μl of the immunoprecipitated DNA and 2% of the reference material were used as templates. The PCR result was normalized using the input DNA, and the specificity of the PCR amplification was confirmed by agarose gel electrophoresis. SOX2 primers sequence was Forward-5′-CGTTCATCGACGAGGCTAAGCG; Reverse-5′-GAGCTG GTCATGGAGTTGTACTGC.

2.13. Dual luciferase reporter assay

The SOX2 promoter luciferase reporter was constructed by Shanghai GenePharma. Luciferase activity assay was performed 24 h after transfection using the Dual-Luciferase Reporter Assay System (Promega) as described by the manufacturer's protocol using the Lumat LB 9507 Luminometer (Promega, USA).

2.14. Western blot analysis, co-immunoprecipitation (Co-IP), flow cytometry

Western blot analysis was used to detect specific protein expression and performed as previously described [29]. Co-immunoprecipitation and flow cytometry were performed as previously described [28].

2.15. Statistical analysis

Statistical analysis was performed using SPSS software. All data are presented as means ± SD unless stated otherwise. Comparisons between different groups were performed using Student's t-test or ANOVA as appropriate. *P* values of 0.05 or lower were considered statistically significant for all experiments.

3. Results

3.1. Combined 4SC-202 and INK128 treatment synergistically inhibits cell growth and self-renewal of OSCC cells

We first determined the effect of combined 4SC-202 and INK128 treatment on the growth of OSCC cells. At 72 h after treatment, we observed decreased viability in cells treated by 4SC-202 or INK128 alone in a dose-dependent manner (Fig. 1A), while combined treatment elicited a synergistic inhibition of cell viability (CI < 1.0) in both chemosensitive(SCC25,CAL33,CAL27,SCC9,SCC15,HSC6 and UM1) and chemoresistant (CAL27R and KV) OSCC cells (Fig. 1A–B and S1A-C). In contrast, neither single nor combined treatment affected non-transformed epithelial cells or fibroblast cells (Fig. 1C), suggesting a cancer cell specific inhibition by 4SC-202 and INK128.

To determine if the drug treatment induce apoptosis, we performed Annexin V staining. We found that combined treatment synergistically induced cell apoptosis in all the OSCC cell lines tested (Fig. 1D and Fig. S1D). Western blot analysis showed that combined treatment increased the protein level of cleaved caspase 3/9 and PARP compared with single treatment or control in CAL33 and CAL27R cells (Fig. S1E). This result suggests that CAL33 and CAL27R impair cell viability through the intrinsic apoptosis pathway.

Next, we addressed if the drug treatment affects self-renewal of OSCC cells. Combined 4SC-202 and INK128 treatment synergistically reduced the $ALDH1^+$ CSCs (Fig. 1E and Fig. S2A) and sphere-forming ability (Fig. 1F and Figs. S2B–C). Notably, combined treatment inhibited sphere formation in CAL33 and CAL27R cells by 70.66% and 81.33%, and colony forming proliferation by 55% and 64%, respectively (Fig. 1G and S2B—C).

To study the effect of combined treatment *in vivo*, we established a subcutaneous tumor model in immunocompromised mice using the CAL33 cells. We did not observe significant difference in body weight of mice among treatment groups (Fig. S1F). However, consistent with the *in vitro* observations in OSCC cells, we found substantially shrunk tumors after combined treatment (407.87 ± 140.89 mm^3) with compared with the single treatment groups (4SC-202: 804.11 ± 466.24 mm^3; INK128: 843 0.81 ± 378.48 mm^3, $P < 0.05$) (Fig. 1H–I).

To determine if combined treatment preferentially targets CSCs *in vivo*, we conducted limiting dilution assay (LDA) to assess the cell propagating capacity. As shown in Fig. 1J, combined treatment significantly suppressed tumor formation after CAL33 cell transplantation compared with single treatment groups.

Taken together, our data indicate that combined 4SC-202 and INK128 treatment synergistically suppresses tumor formation via inducing apoptotic cell death and inhibiting self-renewal of OSCC cells.

3.2. Combined 4SC-202 and INK128 treatment inhibits tumorigenesis of 4NQO induced OSCC

To investigate if combined treatment blocks tumorigenesis of OSCC *in vivo*, we established a rat OSCC model induced with 4-Nitroquinoline (4NQO) and administrated single treatment of 4SC-202, INK128 or cisplatin as well as combined 4SC-202 and INK128 (Fig. 2A). The untreated animals developed lesions starting on the dorsal tongue. By week 22 premalignant dysplastic lesion or squamous cell carcinoma (SCC) developed in the tongue (Fig. 2B). Animals receiving treatment all showed significantly reduced surface area of lesion compared with the control group (Fig. 2C). Notably, histopathological analysis revealed that the percentages of the SCC formation were significantly decreased in the combined treatment (25%) and cisplatin treatment groups (37.5%) compared with 87.5% in the control group (Fig. 2D–E). However, 4SC-202 or INK128 treatment alone showed no significant difference in histological examination compared to the control group (Fig. 2E). These results indicate that combined treatment effectively alleviates OSCC tumorigenesis *in vivo*.

Since cisplatin treatment enriched CSCs [6], we further analyzed the proliferating cells ($Ki67^+$), apoptotic cells (active $caspase\text{-}3^+$) and $ALDH1^+$ cells in OSCC tissue. We found that cisplatin treatment significantly reduced proliferating cells compared with the control, whereas combined treatment dramatically reduced both $Ki67^+$ proliferation cells and $ALDH1^+$ CSCs in OSCC tissue (Fig. 2F–I). Additionally, histopathological examination of liver and kidney tissues among treatment groups showed no changes compared to untreated group (Fig. S3).

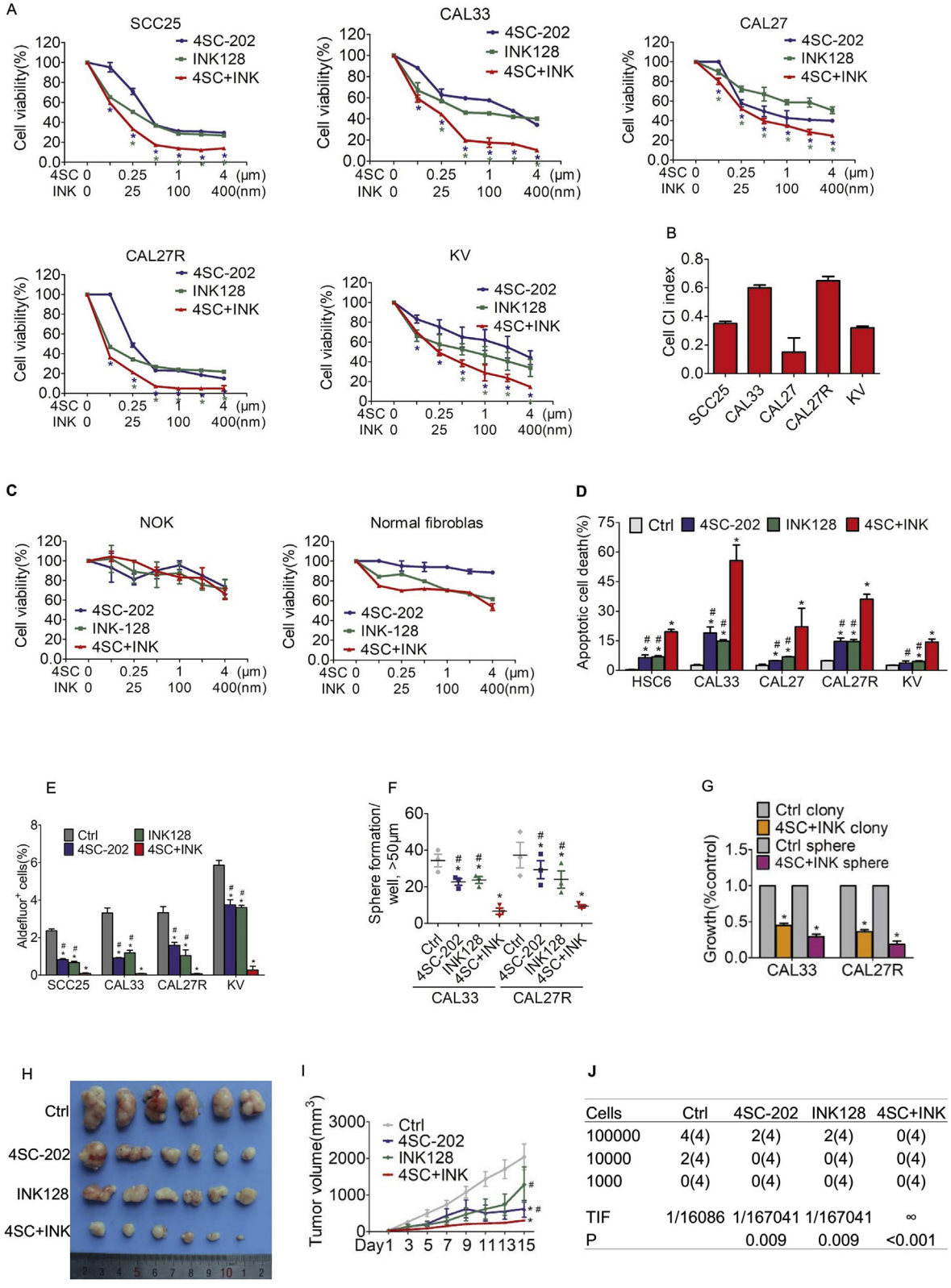

J

Cells	Ctrl	4SC-202	INK128	4SC+INK
100000	4(4)	2(4)	2(4)	0(4)
10000	2(4)	0(4)	0(4)	0(4)
1000	0(4)	0(4)	0(4)	0(4)
TIF	1/16086	1/167041	1/167041	∞
P		0.009	0.009	<0.001

(caption on next page)

3.3. Combined 4SC-202 and mTORC1/C2 treatment inhibits cancer growth in recurrent OSCC in vivo

We sought to evaluate the therapeutic effects of combined treatment on the recurrent OSCC. We established a recurrent OSCC rat model by administering two rounds of drug treatment to induce recurrent premalignant or SCC lesions (Fig. 3A). We found that combined 4SC-202 and INK128 treatment reduced the lesion surface areas ($P < 0.05$) and invasive tumor growth ($P = 0.005$) compared with cisplatin treatment (Fig. 3B–D). These findings are further supported by our immunostaining and histological analysis, which revealed that combined treatment significantly reduced Ki67$^+$ proliferating cells and

Fig. 1. Combined class I HDAC (4SC-202) and mTORC1/C2 (INK128) antagonist synergistically inhibits cell growth and induces cell apoptosis of OSCC *in vitro* and *in vivo*. **(A)** Chemosensitive OSCC cells (SCC25, CAL33 and CAL27) and chemoresistant OSCC cells (CAL27R and KV) were treated with 4SC-202, INK128 or combination at various concentrations for 72 h. Then, cells were analyzed for cellular viability. Values are mean ± SD from three independent experiments. See Supplementary Fig. 1 for additional cell lines. (**B)** Combination index (CI) for each cell lines was calculated using Compusyn software and the CI value was shown as means ± SD. A CI value of less than 1.0 indicates synergy, whereas a CI value larger than 1.0 shows antagonism. A CI value of 1.0 defines additivity. (C) NOK (immortalized oral epithelial cell) and fibroblast cells were treated with 4SC-202, INK128 alone or in combination for 72 h and cell viability were analyzed. Values are mean ± SD from three independent experiments.**(D)** Chemosensitive OSCC cells (CAL33, HSC6 and CAL27) and chemoresistant cells (CAL27R and KV) were treated with indicated drugs for 24 h, stained with Annexin-V/PI and analyzed by flow cytometry. Values are mean ± SD from three independent experiments. **(E)** The proportions of $ALDH^{high+}$ cells among groups were determined by flow cytometry. **(F)** Quantification of 3D sphere formation from different treatment groups. **(G)** Quantification of 3D sphere formation and 2D colony proliferation after 4SC-202 and INK128 combined treatment. **(H)** Mice with CAL33 subcutaneous xenogeneic tumor were treated with 4SC-202 (100 mg/kg), INK128(0.3 mg/kg) or combination daily by oral gavage for 17 days, followed by harvested the tumor. Images showed the xenogeneic tumors among the four groups. **(I)** Tumor volume was measured every 3 days of different groups. Data represent means ± SD, $^{*}P < 0.05$ vs. control, $\#P < 0.05$ vs. 4SC-202 plus INK128. **(J)** In vivo limiting dilution analysis of tumor formation frequency after 4SC-202, INK128 or in combined treatment. The number of tumors arising after the transplantation of different dilutions of cells from different treatment groups was summarized. Estimated frequency of TIF was calculated using the ELDA software. Values are mean ± SD from three independent experiments. $^{*}P < 0.05$ vs. control, $\#P < 0.05$ vs. 4SC-202 plus INK128.

$ALDH1^{+}$ CSCs in recurrent lesions than the single treatment groups ($P < 0.05$, Fig. 3E–F). These results suggest that combined 4SC-202 and INK128 treatment effectively blocks growth of recurrent OSCC *in vivo* through inhibiting cell proliferation and CSCs.

3.4. Combined 4SC-202 and INK128 treatment represses the sex-determining region Y−box 2 (SOX2) gene

To examine the molecular mechanism underlying the synergistic anti-cancer capacity of combined treatment, we analyzed the transcriptome of OSCC cells treated with combined 4SC-202 and INK128. We identified 733 upregulated and 733 downregulated genes after combined treatment, representing over 2-fold increase (Fig. S4A). Kyoto Encyclopedia of Genes and Genomes (KEGG) analysis revealed significant enrichment of signaling networks, including microRNAs in cancer, Hippo signaling, MAPK signaling pathway, stem cells pluripotency, and mTOR signaling pathway (Fig. 4A). We further analyzed differentially expressed genes related with self-renewal (Fig. 4B). Notably, SOX which is essential for stem cells maintenance, was dramatically downregulated. SOX2 protein level in OSCC cells was markedly reduced by the combined treatment, compared with single 4SC-202 or INK128 treatment in OSCC cells (Fig. 4C).

To further examine the role of SOX2 in human OSCC, we assessed SOX2 and ALDH1 protein expression by immunohistochemistry in 80 paired human tissue samples of oral squamous cell carcinomas (OSCC) and their normal adjacent tissues (NAT). The staining index of both SOX2 and ALDH1 were enhanced significantly in OSCC tissues than in NAT ($P < 0.001$, Fig. 4D–E). In addition, our correlation analysis showed a strong association between SOX2 and ALDH1 expression in OSCC tissues (Fig. 4F). To investigate the effect of combined treatment on clinical course of human OSCC, we divided the 80 patients into dichotomous groups based on SOX2 level in OSCC tissues. Patients with high level of SOX2 (staining index ≥ 4) had higher percentage of poorly differentiated tumor, advanced clinical stage and metastatic tumors compared with patients with low level of SOX2 (staining index < 4, Table S2). Our SOX2 ChIP-qPCR data showed that SOX2 occupied the *ALDH1A1* promoter, and this binding was significantly repressed by 4SC-202 or INK128 treatment in CAL33 and CAL27R cells (Fig. 4G and Fig. S4E). Notably, combined treatment further interrupted binding of SOX2 on *ALDH1A1* promoter compared with the single treatment (Fig. 4G).

3.5. SOX2 confers drug resistance to OSCC cells

Next, we sought to address if inhibition of SOX2 is directly linked to the therapeutic effect of combined 4SC-202 and INK128 treatment. We generated the SOX2-overexpressing SCC25 and CAL33 stable cell lines by transducing OSCC cell lines with retroviruses (Fig. 5A and Fig. S5A). SOX2 overexpression significantly attenuated the inhibition of cell viability (Fig. 5B) and $ALDH1^{+}$ CSCs by combined treatment (Fig. 5C and Fig. S5B), suggesting that the combined treatment targets CSCs through inhibiting SOX2.

To further determine if SOX2 mediates chemoresistance of OSCCs, we knocked down SOX2 in cisplatin-resistant CAL27R cells and vincristine (VCR)-resistant KV cells, where SOX2 and ALDH1 proteins were upregulated (Fig. 5D). We found that tumor cell proliferation, $ALDH1^{+}$ cell frequency and sphere-forming ability were significantly decreased in cells with SOX2 knockdown than in vector control cells (Fig. 5E–H and S5C-E).

Moreover, our *in vivo* xenogeneic tumor model showed that SOX2 knockdown substantially reduced the tumor volume at day 27 compared with the control (369.36 mm^3 vs 692 mm^3) (Fig. 5I–J). Importantly, CAL27R cells became sensitive to cisplatin treatment and KV cells became sensitive to VCR treatment (Fig. 5K). These data indicate that SOX2 directly contributes to the chemoresistance of OSCC cells.

3.6. Combined 4SC-202 and INK128 treatment inhibits SOX2 through cooperative inhibition at translational level

To elucidate the molecular mechanism by which the combined treatment synergistically inhibited SOX2 expression, we analyzed transcriptome of CAL33 cells with combined treatment. RNA-Seq analysis showed that combined treatment dramatically upregulated 12 miRNAs by > 6-fold compared with the untreated cells (Fig. 6A). To identify candidate miRNAs targeting SOX2, we used targeting algorithms (TargetScan and microRNA.org) combined with microRNA data and identified two miRNAs, miR-429 and miR-1181. As shown in Fig. 6B, both miR-429 and miR-1181 were bound to the 3′UTR of SOX2. We further performed qRT-PCR and confirmed that miR-429 and miR-1181 were markely unregulated by 4SC-202 (Fig. 6C), whereas INK128 had no effect on their expression (Fig. S4C).

To validate interaction between miRNA and SOX2, we conducted luciferease reporter assay in CAL27R and CAL33 cells. We cloned the SOX2 3' UTR fragment containing the wild type or mutated sequence bound by miR-429 and miR-1181 into the luciferase reporter (Fig. S4D). As shown in Fig. 6D, both miR-429 and miR-1181 treatment reduced the luciferase activity. However, mutations in the miR-429 or miR-1181 binding sites resulted in a complete restoration of the luciferase activity, suggesting that miR-429 and miR-1181 suppressed SOX2 transcription by directly binding to SOX2.

Since 4SC-202 belongs to class I HDAC inhibitors which upregulate target genes through promoting histone acetylation near the target gene transcription start site (Fig. S4B), we hypothesized that 4SC-202 activates miR-429 and miR-1181 genes via histone acetylation. Our ChIP-qPCR revealed that 4SC-202 enhanced the active histone marks H3ac, H4ac, H3K9ac and H3K27ac in miR-429 gene loci, and H3ac, H4ac and H3K27ac in miR-1181 gene loci (Fig. 6E).

Next, we examined the molecular mechanism of INK128. We found that INK128 inhibited phosphorylation of AKT (a substrate of mTORC2) and 4E-BP1 (a substrate of mTORC1), while 4SC-202 showed no effects

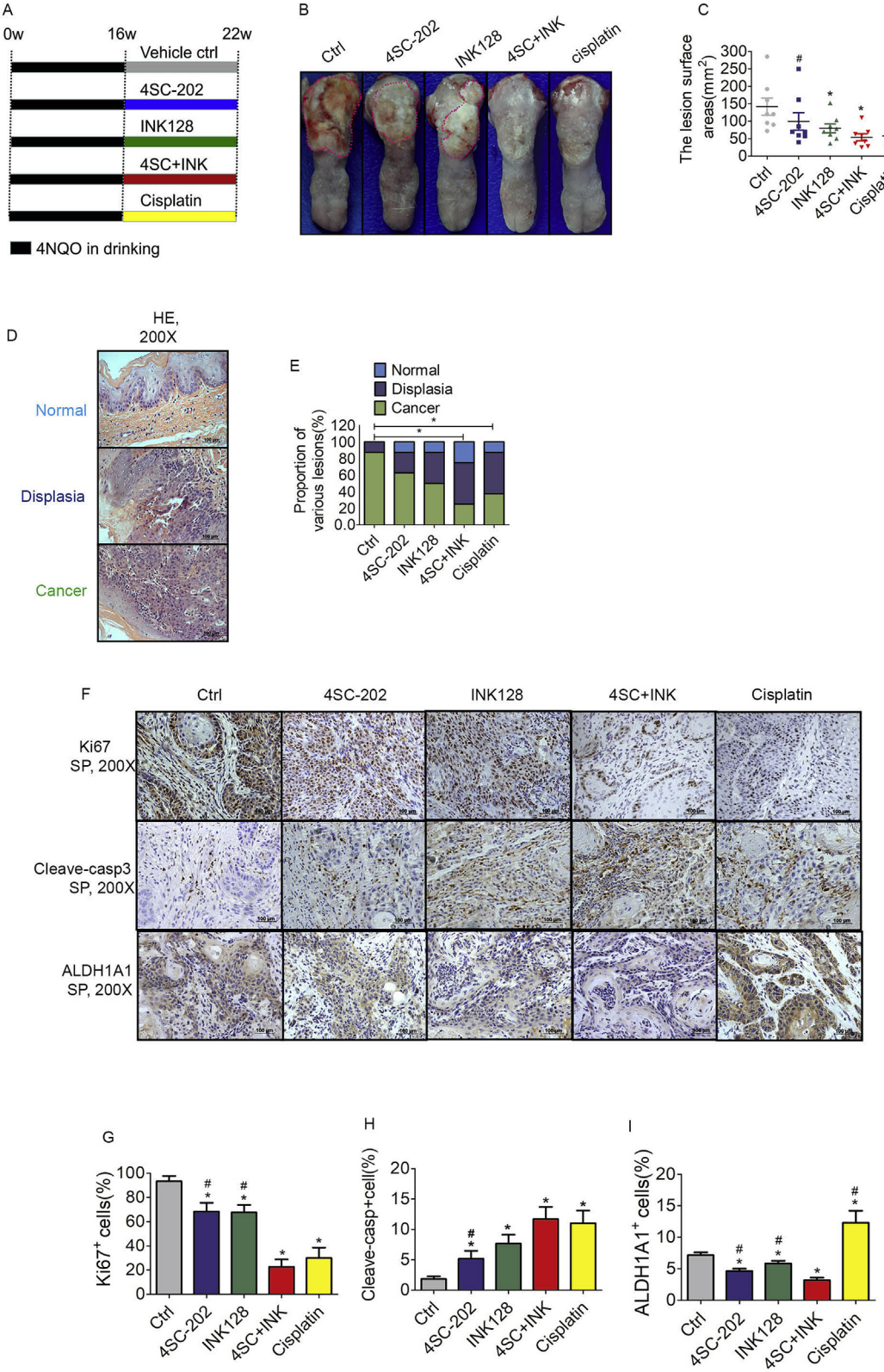

Fig. 2. Combined class I HDAC (4SC-202) and mTORC1/C2 (INK128) blocked the tumorigenesis of OSCC tissue *in vivo*. **(A)** Schematic overview of the experimental design. Briefly, rat OSCC was induced by 4NQO and rats were randomly divided into five experimental groups as follows: vehicle control, 4SC-202, INK128, cisplatin, and 4SC-202 plus INK128. n = 8 for each group. **(B)** Representative image of tongue lesions at 22 weeks after treatment. **(C)** Quantification of lesion areas visible in the tongue from different treatment groups. **(D)** Representative H&E images of rat tongue dysplasia and SCC. Scale bars, 100 μm. **(E)** Quantification of the area ratio of normal, dysplasia and SCC tissues in the five groups. **(F)** Representative immunostaining images for Ki67, cleaved caspase-3 and ALDH1 in OSCC tissue. Scale bars, 100 μm. **(G-I)** Quantification of $Ki67^+$, $Casp3^+$ and $ALDH1^+$ cells in OSCC tissue. $^*P < 0.05$ vs. control, $\#P < 0.05$ vs. 4SC-202 plus INK128.

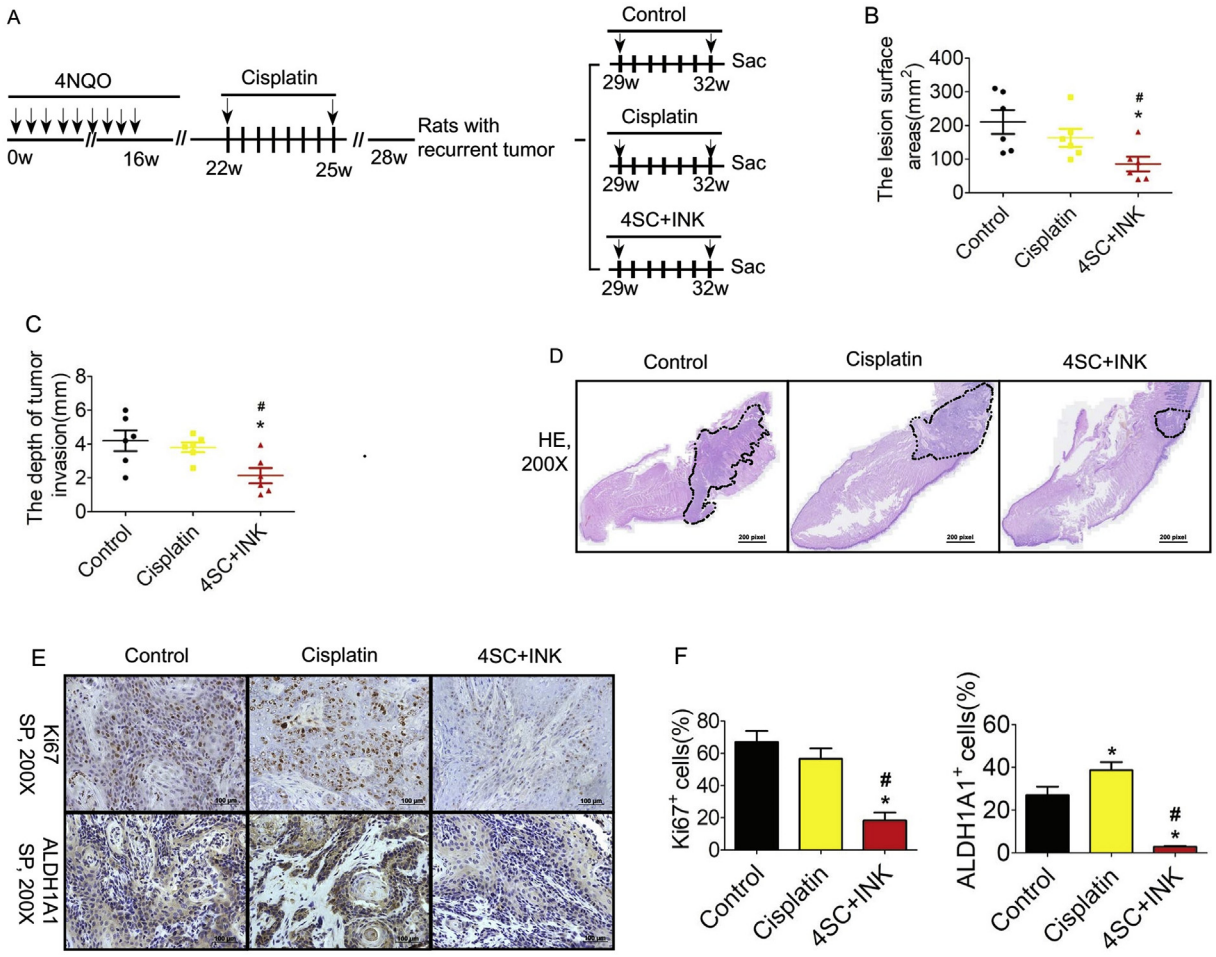

Fig. 3. Combined class I HDAC (4SC-202) and mTORC1/C2 (INK128) antagonist inhibited cancer growth in recurrent OSCC *in vivo*. **(A)** Schematic overview of the experimental design. Briefly, after the first round of cisplatin treatment, rats were maintained for 4 additional weeks. Rats with recurrent SCC lesion were divided into 3 groups: vehicle control, cisplatin and 4SC-202 plus INK128 treatment and received a second round of treatment. At the end of the experiment, all rats were sacrificed and tongue lesions were harvested within one day. **(B)** Quantification of lesion areas visible in the tongue from different treatment groups. Data represent means ± SD, n = 6 for each group. **(C)** Quantification of the depth of tumor invasion in different treatment groups. Data represent means ± SD, n = 6 for each group. **(D)** Representative histological images of human OSCC in rats after treatment. **(E)** Representative immunostaining images of Ki67 and ALDH1 in OSCC after different treatment. Scale bars, 100 mm. **(F)** Quantification of $Ki67^+$ and $ALDH1^+$ cancer stem cells in lesions after different treatment. $^*P < 0.05$ vs. control, $\#P < 0.05$ vs. cisplatin-treated group.

(Fig. 7A). Non-phosphorylated 4E-BPs interacte strongly with translation initiation factor 4E (eIF4E), thereby preventing cap-dependent mRNA translation; whereas phosphorylated 4E-BPs bind weakly to eIF4E and do not interfere with the process of translation [30]. Co-immunoprecipitation showed that INK128 strengthened the interaction between 4E-BP1 and eIF4E (Fig. 7B). Further RNA immunoprecipitation (RIP) assay showed that INK128 treatment weakened physical interaction of eIF4E with SOX2 mRNA compared with the vehicle control in CAL33 and CAL27R cells, suggesting that INK128 inhibited SOX2 translation by promoting eIF4E capping of SOX2 mRNA (Fig. 7C–D).

4. Discussion

In this study, we investigated the effect of combined 4SC-202 and INK128 treatment for OSCC. Our findings demonstrate that combined treatment synergistically inhibited cell growth, sphere-forming ability, $ALDH1^+$ CSCs and *in vivo* tumor formation in rat OSCC model induced by 4NQO. Moreover, combined treatment effectively inhibited the growth of recurrent OSCC *in vitro* and *in vivo*. Mechanistically, we found that 4SC-202 and INK128 repressed SOX2 expression through miRNA-mediated translational repression and preventing cap-dependent mRNA translation, respectively. SOX2 was upregulated in advanced OSCC and metastatic tumors and contributed to drug resistance of OSCC, as shown by the SOX2 overexpression and knockdown experiments. SOX2 overexpression significantly attenuated the inhibition of cell viability and $ALDH1^+$ CSCs by the combined treatment; whereas SOX2 knockdown effectively alleviated the drug resistance of OSCCs. Taken together, here we report for the first time that combination of 4SC-202 and INK128 treatment effectively inhibits cell growth and CSCs in OSCCs by repressing SOX2 translationally.

Previous preclinical studies have shown that the combined HDACi and PI3K/mTOR antagonist treatment synergistically promoted tumor regression in medulloblastoma or lymphoma (DLBCL) cells [31–33]. Since overexpression of class I HDAC was associated with advanced OSCC or poor prognosis [13], we selected a novel class I HDAC inhibitor 4SC-202. The combined 4SC-202 and INK128 treatment blocked OSCC tumorigenesis in the OSCC model induced by 4NQO. Notably, the combined treatment exerted a synergistic effect on reducing CSCs during tumorigenesis of OSCCs. In contrast, the conventional chemotherapeutic agent cisplatin increased CSC population in OSCCs, leading to drug resistance and relapse of tumor in remote or local area [6,7]. These findings indicate that combined 4SC-202 and INK128 treatment is more effective and promising than conventional chemotherapy. Furthermore, our results demonstrate that the combined

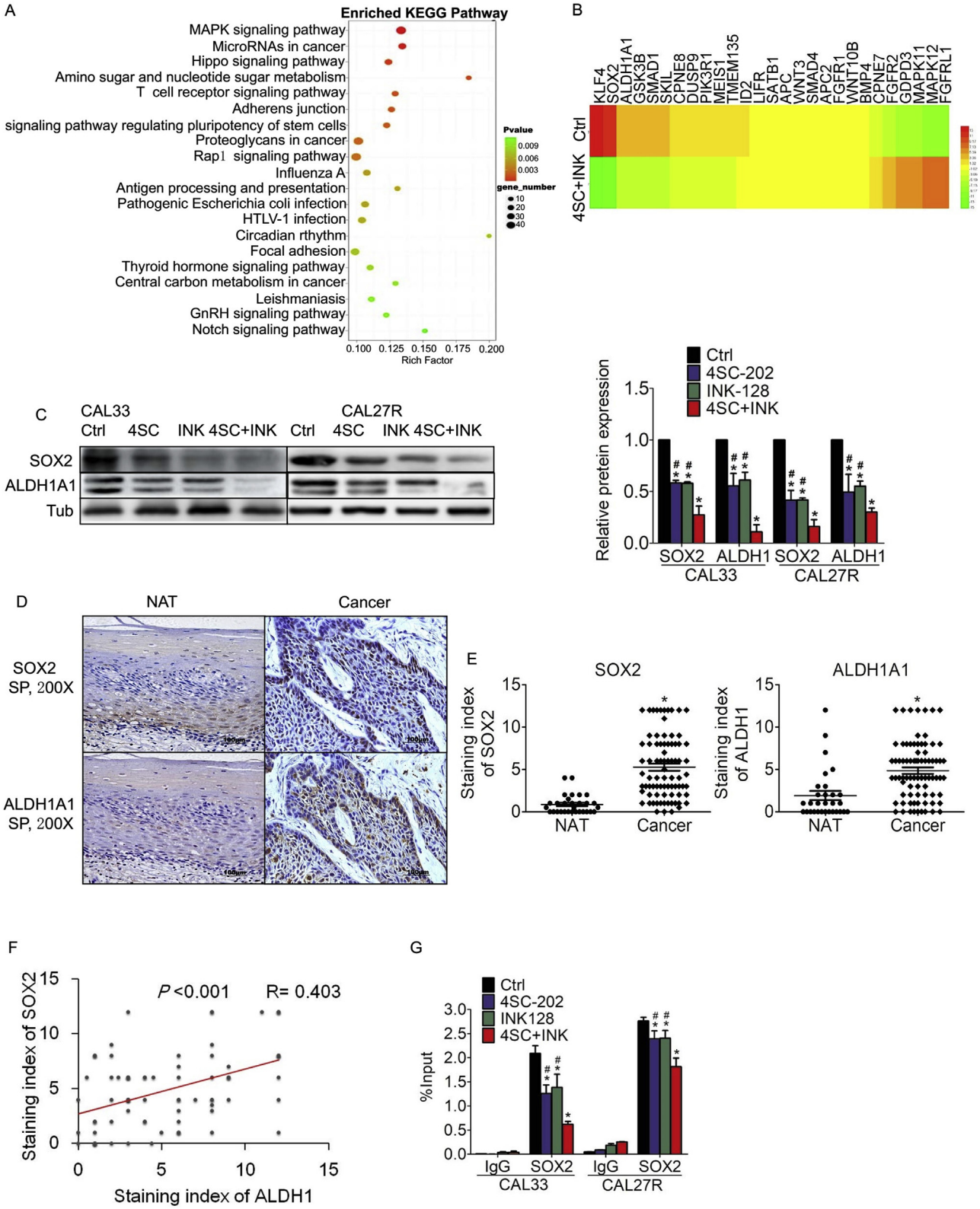

Fig. 4. SOX2 was regulated by both 4SC-202 and INK128 in OSCC. **(A)** KEGG analysis was used to generate a list of enriched biofunctions and pathways affected by combined 4SC-202 and INK128 treatment in CAL33 cells. Statistical significance was calculated by a two-sided modified Kolmogorov-Smirnov permutation test. **(B)** The heatmap depicts standardized expression (Z-scores) of key genes along with cell proliferation, apoptosis and stem cell-associated genes after 4SC plus INK treatment. **(C)** SOX2 and ALDH1 protein levels after 4SC-202, INK128 or combined treatment in OSCC cells. **(D)** Increased SOX2 and ALDH1 expression in human OSCC samples (n = 80) and noncancerous adjacent tissues (NAT, n = 30). Representative histochemistry images (100x) for SOX2 and ALDH1 staining are shown. Scale bars, 100 μm. **(E)** The quantification of SOX2 and ALDH1 expression in human OSCC tissue and NAT. **(F)** Correlation analysis between SOX2 and ALDH1 expression in the human OSCC tissue. **(G)** ChIP-qPCR analysis using SOX2 antibodies to examine the binding of SOX2 protein to ALDH1A1 promoter after 4SC-202, INK128 or combined treatment.*$P < 0.05$ vs. control, #$P < 0.05$ vs. 4SC-202 plus INK128.

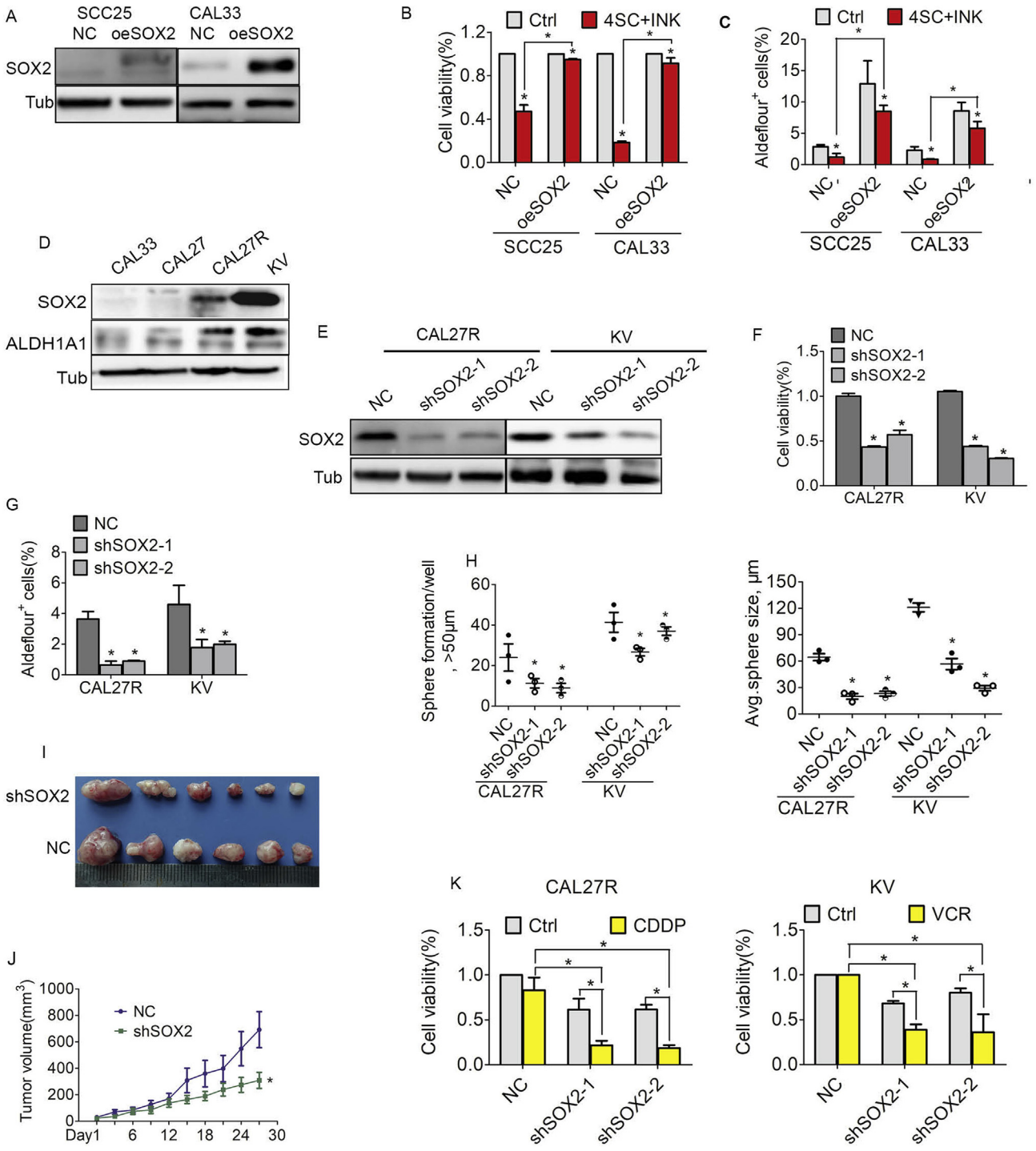

Fig. 5. SOX2 regulated chemo-sensitive properties of OSCC cells. **(A)** SOX2 expression in SCC25 and CAL33 cells after transduced with retroviruses expressing SOX2. **(B)** Cellular viability analysis in SOX2 overexpressed OSCC cells with combined 4SC-202 and INK128 treatment. **(C)** Percentages of ALDH1^{high+} population in SOX2 overexpressed OSCC cells with combined 4SC-202 and INK128 treatment. **(D)** Western blot analysis of SOX2 and ALDH1 expression in CAL33,CAL27 and drug-resistant OSCC cells. Tubulin was used as endogenous loading control. **(E)** SOX2 expression in CAL27R and KV cells after transduced with retroviruses expressing SOX2 siRNA. **(F)** Cellular viability analysis in SOX2 knowdown CAL27R and KV cells. **(G)** Percentages of ALDH1^{high+} population in SOX2 knowdown CAL27R and KV cells. **(H)** Sphere formation analysis in SOX2 knowdown CAL27R and KV cells. **(I)** In vivo xenogeneic tumor model was carried out by subcutaneous injection of SOX2 knockdown stable KV cells. The xenogeneic tumor images formed by subcutaneously injected SOX2 knowdown KV cells or KV control cells. **(J)** Tumor volume was measured and calculated every 3 days of different groups. Data represent means ± SD. **(K)** Enhanced drug sensitivity of CAL27R cells to cisplatin and KV cells to VCR after transduced with retroviruses expressing SOX2 siRNA by using CCK8 assay. *$P < 0.05$ vs. control, #$P < 0.05$ vs. 4SC-202 plus INK128.

treatment did not affect the growth of normal epithelia or fibroblast cells and had no liver or renal toxicity, highlighting its therapeutic potentials.

This study further reveals that the combined treatment suppresses tumorigenesis of OSCCs through SOX2, a member of the SRY-related HMG-box (SOX) transcription factor family, which plays a critical role in self-renewal or pluripotency of stem cells [34]. Upregulation of SOX2 was identified in a variety of cancers, such as skin squamous cell

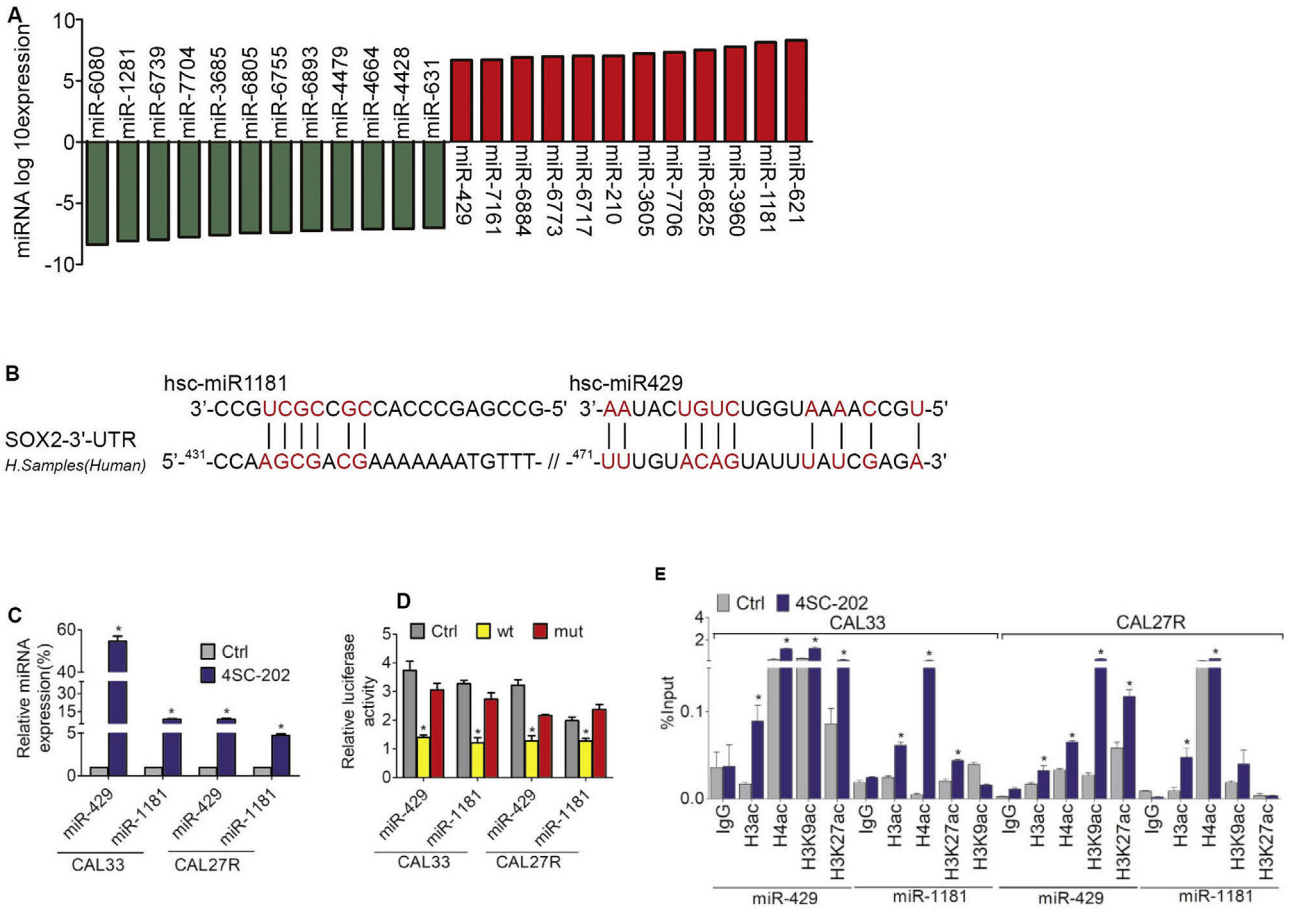

Fig. 6. Mechanism of 4SC-202-induced downregulation of SOX2. (**A**)RNA-Seq analysis of differentially expressed microRNA that changed more than 6-fold in CAL33 cells after combined 4SC-202 and INK128 treatment **(B)** Nucleotides analysis in the miR-1181 and miR-429 seed sequence and the 3′-UTR region of SOX2. **(C)** QRT-PCR analysis of miR-429 and miR-1181 expression after 4SC-202 treatment. **(D)** The effect of miRNA mimics on the luciferase activities of the construct containing the wild-type (wt) or mutant-type (mut) 3′-UTR fragments in CAL33 and CAL27R cells. **(E)** ChIP-qPCR analysis of active histone marks H3ac, H4ac, H3K9ac and H3K27ac at miR-429 and miR-1181 gene loci after 4SC-202 treatment.

carcinoma, lung squamous cell carcinoma and colorectal cancer [35–37]. However, the role of SOX2 in OSCCs remained controversial. SOX2 promoted the invasiveness of OSCC cells and high SOX2 protein levels were associated with poor prognosis of OSCC patients [38,39]. In contrast, other studies showed that low SOX2 expression in OSCC tissues was significantly associated with poor survival [40], whereas SOX2 activation was correlated to improved prognosis in patients [41]. Our results show that SOX2 was upregulated in human OSCC and high level of SOX2 was associated with poorly differentiated and metastatic tumor as well as advanced clinical stage, suggesting the oncogenic property of SOX2. Notably, the combined treatment downregulated SOX2 in OSCC, and subsequently inhibited its binding to ALDH1A1 promoter. SOX2 overexpression partially blocked growth inhibition by combined treatment. Our mechanistic study further showed that the class I HDACi 4SC-202 suppressed SOX2 by increasing the active histone marks including H3ac, H4ac, H3K9ac and H3K27ac at the gene loci of miR-429 and miR-1181, Both miR-429 and miR-1181 targeted SOX2 and induced miRNA-mediated translational repression. Additionally, we found that INK128 strengthened the interaction between non-phosphorylated 4E-BP1 and eIF4E, thereby promoted EIF4E capping of SOX2 mRNA to block SOX2 translation. These results indicate that combined 4SC-202 and INK128 treatment could simultaneously inhibit SOX2 by two distinct mechanisms, which synergistically contribute to therapeutic efficacy for OSCC.

The main challenge in OSCC treatment is cancer recurrence due to development of cisplatin resistance [6]. Growing evidences shows that CSCs, also known as tumor-initiating cells, are responsible for tumor initiation and drug resistance, which leads to cancer recurrence [8]. In our result, although both cisplatin and combined 4SC-202 and INK128 treatment reduced the SCC formation, the effect of latter is more profound. Compared with cisplatin, combination treatment effectively blocked growth of recurrent OSCC. Besides, ALDH1 is used as a CSCs marker in many types of cancer [8]. Our data showed that cisplatin treatment inhibited cell proliferation but enriched ALDH1$^+$ CSCs population in two OSCC models induced by 4NQO, while combined treatment effectively inhibited both cell proliferation and ALDH1$^+$ CSCs. Moreover, results from SOX2 overexpression and knockdown experiments indicate that SOX2 is the key factor responsible for the chemoresistance of OSCCs. Overall, our findings in recurrent OSCC model induced by 4NQO support that targeting both HDAC and mTORC1/C2 is an effective therapy for OSCCs to overcome the cisplatin-induced drug resistance through repressing SOX2 expression.

In summary, we have demonstrated that the concomitant inhibition of class I HDAC and mTORC1/C2 synergistically blocks the initiation of OSCC and overcomes chemoresistance by downregulating SOX2 expression through miR-429/miR-1181-mediated translational repression and preventing cap-dependent mRNA translation, respectively (Fig. 7E). Our studies identify a promising therapeutic combination that are potentially applicable in other solid tumors, such as skin and lung cancer. We have provided evidences for the principle of selectively targeting self-renewing capacity of cancer cells as effective combinational therapies.

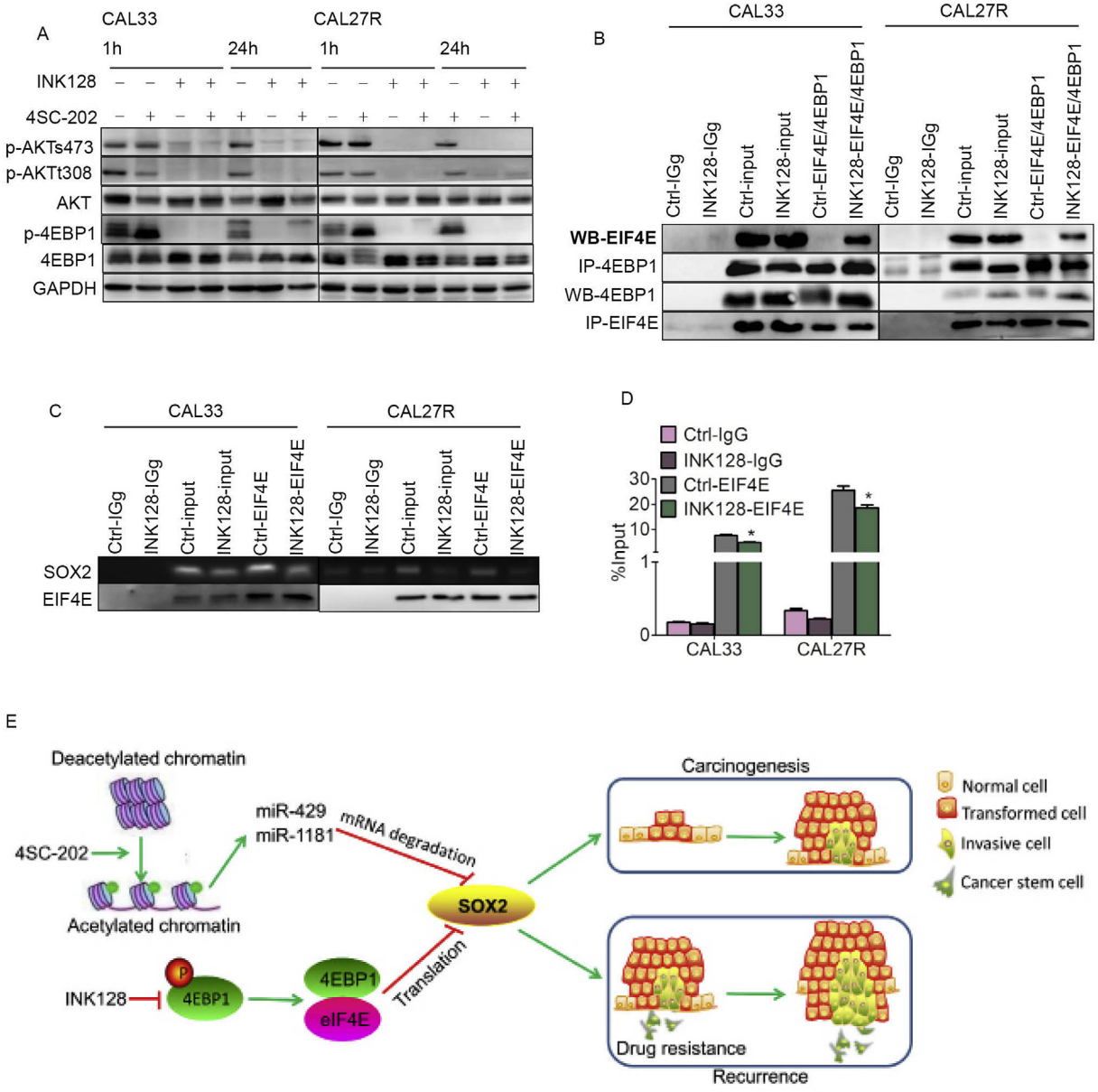

Fig. 7. Mechanism of INK128-induced downregulation of SOX2. a(**A)** The expression of p-AKT (T308), p-AKT(S473) and p-4EBP1 after 4SC-202, INK128 or combined treatment. (**B)** Co-immunoprecipitation analysis of the 4EBP1 and eIF4E binding after INK128 treatment. (**C-D)** RNA immunoprecipitation analysis of SOX2 expression after INK128 treatment using eIF4E specific antibodies. Results represent means ± SD of three experiments performed in triplicate. *$P < 0.05$ versus control, #$P < 0.05$ versus 4SC-202 plus INK128.(**E**)The schematic diagram shows the mechanism that combined class I HDAC and mTORC1/C2 inhibition downregulates SOX2 through cooperative inhibition at translational level to suppress the carcinogenesis and recurrence of OSCC.

Acknowledgements

We thank the support by grants from the National Natural Science Foundation of China (No. 81870769, 81671000, J. Xia) and the Science and Technology Program of Guangzhou, China (No. 201803010019, J. Xia), and thank Professor Xiaohua Chen at the department of oral pathology for histopathological diagnosis, and Professor Meng Zhao at Zhongshan Medical School for animal experiment.

Appendix A. Supplementary data

Supplementary data to this article can be found online at https://doi.org/10.1016/j.canlet.2019.04.010.

Conflicts of interest

The authors declare no conflicts of interest.

References

[1] R.L. Siegel, K.D. Miller, A. Jemal, Cancer statistics, 2018, CA. Cancer, J. Clin. 68 (2018) 7–30.
[2] J. Ali, B. Sabiha, H.U. Jan, S.A. Haider, A.A. Khan, S.S. Ali, Genetic etiology of oral cancer, Oral Oncol. (2017) 23–28.
[3] N. Vigneswaran, M.D. Williams, Epidemiologic trends in head and neck cancer and aids in diagnosis, Oral, Maxillofac. Surg. Clin. North. Am. 26 (2014) 123–141.
[4] N. Sinevici, J. O'sullivan, Oral cancer: deregulated molecular events and their use as biomarkers, Oral, Oncol. 61 (2016) 12–18.
[5] J. Thariat, S. Vignot, A. Lapierre, A.T. Falk, J. Guigay, E.V. Obberghen-Schilling, et al., Integrating genomics in head and neck cancer treatment: promises and pitfalls, Crit. Rev. Oncol. Hematol. 95 (2015) 397–406.
[6] C. Nör, Z. Zhang, K.A. Warner, L. Bernardi, F. Visioli, J.I. Helman, et al., Cisplatin induces Bmi-1 and enhances the stem cell fraction in head and neck cancer,

Neoplasia 16 (2014) 137–146.
[7] P. Jiang, C. Xu, M. Zhou, H. Zhou, W. Dong, X. Wu, et al., RXRα-enriched cancer stem cell-like properties triggered by CDDP in head and neck squamous cell carcinoma (HNSCC), Carcinogenesis 39 (2018) 252–262.
[8] L.T.H. Phi, I.N. Sari, Y.G. Yang, S.H. Lee, N. Jun, K.S. Kim, et al., Cancer stem cells (CSCs) in drug resistance and their therapeutic implications in cancer treatment, Stem Cell. Int. 2018 (2018) 5416923.
[9] L. MacDonagh, S.G. Gray, E. Breen, S. Cuffe, S.P. Finn, K.J. O'Byrne, et al., BBI608 inhibits cancer stemness and reverses cisplatin resistance in NSCLC, Cancer Lett. 428 (2018) 117–126.
[10] M.E. Prince, R. Sivanandan, A. Kaczorowski, G.T. Wolf, M.J. Kaplan, P. Dalerba, et al., Identification of a subpopulation of cells with cancer stem cell properties in head and neck squamous cell carcinoma, Proc. Natl. Acad. Sci. Unit. States Am. 104 (2007) 973–978.
[11] R.M. Castilho, C.H. Squarize, L.O. Almeida, Epigenetic modifications and head and neck cancer: implications for tumor progression and resistance to therapy, Int. J. Mol. Sci. 18 (2017) E1506 pii.
[12] H.P. Chen, Y.T. Zhao, T.C. Zhao, Histone deacetylases and mechanisms of regulation of gene expression, Crit. Rev. Oncog. 20 (2015) 35–47.
[13] H.H. Chang, C.P. Chiang, H.C. Hung, C.Y. Lin, Y.T. Deng, M.Y.P. Kuo, Histone deacetylase 2 expression predicts poorer prognosis in oral cancer patients, Oral Oncol. 45 (2008) 610–614.
[14] M.R. Ramsey, L. He, N. Forster, B. Ory, L.W. Ellisen, Physical association of HDAC1 and HDAC2 with p63 mediates transcriptional repression and tumor maintenance in squamous cell carcinoma, Cancer Res. 71 (2011) 4373–4379.
[15] P.T. Bhaskar, N. Hay, The two TORCs and akt, Dev. Cell 12 (2007) 487–502.
[16] F. Dogan, C.B. Avci, Correlation between telomerase and mTOR pathway in cancer stem cells, Gene 641 (2018) 235–239.
[17] V.W.Y. Lui, M.L. Hedberg, H. Li, B.S. Vangara, K. Pendleton, Y. Zeng, et al., B.R. Gilbert, Frequent mutation of the PI3K pathway in head and neck cancer defines predictive biomarkers, Cancer Discov. 3 (2013) 761–769.
[18] R.V. Broek, S. Mohan, D.F. Eytan, Z. Chen, C.V. Waes, The PI3K/Akt/mTOR axis in head and neck cancer: functions, aberrations, cross-talk, and therapies, Oral Dis. 21 (2015) 815–825.
[19] M. Fu, F. Wan, Z. Li, F. Zhang, 4SC-202 activates ASK1-dependent mitochondrial apoptosis pathway to inhibit hepatocellular carcinoma cells, Biochem. Biophys. Res. Commun. 471 (2016) 267–273.
[20] S.M. Messerli, M.M. Hoffman, E.Z. Gnimpieba, H. Kohlhof, R. D Bhardwaj, 4SC-202 as a potential treatment for the pediatric Brain tumor medulloblastoma, Brain Sci. 7 (2017) 147.
[21] M. Pinkerneil, M.J. Hoffmann, H. Kohlhof, W.A. Schulz, G. Niegisch, Evaluation of the therapeutic potential of the novel isotype specific HDAC inhibitor 4SC-202 in urothelial carcinoma cell lines, Targeted Oncol. 11 (2016) 783–798.
[22] Z. Huang, S. Wang, H. Min, J. Li, L.S. Qin, D. Li, Pre-clinical characterization of 4SC-202, a novel class I HDAC inhibitor, against colorectal cancer cells, Tumour. Biol. 37 (2016) 10257–10267.
[23] B.V. Tresckow, C. Sayehli, W.E. Aulitzky, M.E. Goebeler, M. Schwab, E. Braz, et al., Phase I study of domatinostat (4SC-202), a class I histone deacetylase inhibitor in patients with advanced hematological malignancies, Eur. J. Haematol. 102 (2019) 163–173.
[24] Z.G. Liu, J. Tang, Z. Chen, H. Zhang, H. Wang, J. Yang, et al., The novel mTORC1/2 dual inhibitor INK128 enhances radiosensitivity of breast cancer cell line MCF-7, Int. J. Oncol. 49 (2016) 1039–1045.
[25] M.R. Janes, C. Vu, S. Mallya, M.P. Shieh, J.J. Limon, L.S. Li, et al., Efficacy of the investigational mTOR kinase inhibitor MLN0128/INK128 in models of B-cell acute lymphoblastic leukemia, Leukemia 27 (2013) 586–594.
[26] T.J. Hayman, A. Wahba, B.H. Rath, H. Bae, T. Kramp, U.T. Shankavaram, et al., The ATP-competitive mTOR inhibitor INK128 enhances in vitro and in vivo radiosensitivity of pancreatic carcinoma cells, Clin. Cancer Res. 20 (2014) 110–119.
[27] Z. Zhuang, N. Xie, J. Hu, P. Yu, C. Wang, X. Hu, et al., Interplay between ΔNp63 and miR-138-5p regulates growth, metastasis and stemness of oral squamous cell carcinoma, Oncotarget 8 (2017) 21954–21973.
[28] H. Wang, X. Liang, M. Li, X. Tao, S. Tai, Z. Fan, et al., Chemokine (CC motif) ligand 18 upregulates Slug expression to promote stem-cell like features by activating the mammalian target of rapamycin pathway in oral squamous cell carcinoma, Cancer Sci. 108 (2017) 1584–1593.
[29] Y. Wang, X. Zhang, Z. Wang, Q. Hu, J. Wu, Y. Li, et al., LncRNA-p23154 promotes the invasion-metastasis potential of oral squamous cell carcinoma by regulating Glut1-mediated glycolysis, Cancer Lett. 434 (2018) 172–183.
[30] D. Peter, C. Igreja, R. Weber, L. Wohlbold, C. Weiler, L. Ebertsch, et al., Molecular architecture of 4E-BP translational inhibitors bound to eIF4E, Mol. Cell. 57 (2015) 1074–1087.
[31] M. Rahmani, M.M. Aust, E.C. Benson, L. Wallace, J. Friedberg, S. Grant, PI3K/mTOR inhibition markedly potentiates HDAC inhibitor activity in NHL cells through BIM- and MCL-1-dependent mechanisms in vitro and in vivo, Clin. Cancer Res. 20 (2014) 4849–4860.
[32] C.F. Malone, C. Emerson, R. Ingraham, W. Barbosa, S. Guerra, H. Yoon, et al., mTOR and HDAC inhibitors converge on the TXNIP/thioredoxin pathway to cause catastrophic oxidative stress and regression of RAS-driven tumors, Cancer Discov. 7 (2017) 1450–1463.
[33] Y. Pei, K.W. Liu, J. Wang, A. Garancher, R. Tao, L.A. Esparza, et al., HDAC and PI3K antagonists cooperate to inhibit growth of MYC-driven medulloblastoma, Cancer Cell 29 (2016) 311–323.
[34] C. Deluz, E.T. Friman, D. Strebinge, A. Benke, M. Raccaud, A. Callegari, et al., A role for mitotic bookmarking of SOX2 in pluripotency and differentiation, Genes Dev. 30 (2016) 2538–2550.
[35] S. Boumahdi, G. Driessens, G. Lapouge, S. Rorive, D. Nassar, M. Le Mercier, et al., SOX2 controls tumour initiation and cancer stem-cell functions in squamous-cell carcinoma, Nature 511 (2014) 246–250.
[36] A. Mukhopadhyay, K.C. Berrett, U. Kc, P.M. Clair, S.M. Pop, S.R. Carr, et al., Sox2 cooperates with lkb1 loss in a mouse model of squamous cell lung cancer, Cell Rep. 8 (2014) 40–49.
[37] J. Zheng, L. Xu, Y. Pan, S. Yu, H. Wang, D. Kennedy, et al., Sox2 modulates motility and enhances progression of colorectal cancer via the Rho-ROCK signaling pathway, Oncotarget 8 (2017) 98635–98645.
[38] A. Schröck, M. Bode, F.J. Göke, P.M. Bareiss, R. Schairer, H. Wang, et al., Expression and role of the embryonic protein SOX2 in head and neck squamous cell carcinoma, Carcinogenesis 35 (2014) 1636–1642.
[39] L. Du, Y. Yang, X. Xiao, C. Wang, X. Zhang, L. Wang, et al., Sox2 nuclear expression is closely associated with poor prognosis in patients with histologically node-negative oral tongue squamous cell carcinoma, Oral Oncol. 47 (2011) 709–713.
[40] L. Züllig, M. Roessle, C. Weber, N. Graf, S.K. Haerle, W. Jochum, et al., High sex determining region Y-box 2 expression is a negative predictor of occult lymph node metastasis in early squamous cell carcinomas of the oral cavity, Eur. J. Cancer 49 (2013) 1915–1922.
[41] J.H. Chung, J.R. Jung, A.R. Jung, Y.C. Lee, M. Kong, J.S. Lee, et al., SOX2 activation predicts prognosis in patients with head and neck squamous cell carcinoma, Sci. Rep. 8 (2018) 1677.